Mesoscale hydrodynamics simulations of attractive rod-like colloids in shear flow

2008 J. Phys.: Condens. Matter 20 404209

(http://iopscience.iop.org/0953-8984/20/40/404209)

J. Phys.: Condens. Matter **20** (2008) 404209 (11pp) doi:10.1088/0953-8984/20/40/404209

Mesoscale hydrodynamics simulations of attractive rod-like colloids in shear flow

M Ripoll, R G Winkler, K Mussawisade and G Gompper

Institut für Festkörperforschung, Forschungszentrum Jülich, D-52425 Jülich, Germany

E-mail: m.ripoll@fz-juelich.de

Received 5 May 2008
Published 10 September 2008
Online at stacks.iop.org/JPhysCM/20/404209

Abstract

Suspensions of rod-like colloids show in equilibrium an isotropic–nematic coexistence region, which depends on the strength of an attractive interaction between the rods. We study the behavior of this system in shear flow for various interaction strengths. A hybrid simulation approach is employed, which consists of a mesoscale particle-based hydrodynamics technique (multi-particle collision dynamics) for the solvent and molecular dynamics simulations for the colloidal rods. The shear flow induces alignment in the initially isotropic phase, which generated an additional free volume around each rod and causes the densification of the isotropic phase at the expense of an erosion of the initially nematic phase. Furthermore, the nematic phase exhibits a collective rotational motion. The associated rotational time decreases linearly in $1/\dot{\gamma}$ with increasing shear rate $\dot{\gamma}$, and increases with increasing attraction strength between the rods. The density difference between these two regions at different shear rates allows us to determine the binodal line of the phase diagram. For large applied shear rates, the difference between the phases disappears in favor of a homogeneous flow-aligned state.

(Some figures in this article are in colour only in the electronic version)

1. Introduction

Many soft-matter systems are characterized by a mesoscopic structural length scale which implies a large structural relaxation time, tunability of the interactions between the mesoscopic building blocks, the importance of thermal fluctuations and hydrodynamic interactions, and the sensitivity to external fields and the ubiquity of non-equilibrium conditions. Dense suspensions of rod-like colloids in aqueous solution, containing polymer chains as depletion agents, present an ideal model system to study the interplay of all these different physical mechanisms to determine the non-equilibrium behavior of soft matter under shear flow.

It is well known that rod-like colloids with sufficiently large aspect ratios show a transition from the isotropic to the nematic phase with increasing colloid volume fraction ϕ, where the nematic phase is characterized by quasi-long-range orientational order of the long axes of the rods, but short-range positional order of their centers of mass [1–3]. This transition can be predicted theoretically at different volume fractions as a function of the aspect ratio L/d, where L is the rod length and d the rod diameter [4, 5]. Computer simulations of spherocylinders qualitatively confirm this result [6, 7]. However, the region of isotropic–nematic coexistence is very narrow. The coexistence region widens when there is an attractive interaction among the colloids [8]. Experimentally this is achieved by adding a short, water-soluble polymer, which induces an attractive depletion interaction among colloids with a strength proportional to the polymer concentration [8].

Much less is known about the non-equilibrium behavior of suspensions of rod-like colloids in shear flow. In the dilute limit, rods display a tumbling motion with a frequency ω. The average inclination angle of the rod direction with the flow, the scaled tumbling frequency $\omega/\dot{\gamma}$, and other quantities, are found to depend on the shear rate $\dot{\gamma}$, the solvent viscosity η, the rod length L and the rod diameter d in a scaling form with the Peclet number $Pe = \dot{\gamma}/D_r(L, d, \eta)$ as scaling variable, where D_r is the rotational diffusion constant of a rod-like colloid [9, 10].

At high colloid volume fractions, in the *nematic phase*, the rotation of a rod is hindered by the presence of its neighbors. Individual rods still tumble, but with a much smaller frequency than free rods. However, in dense suspensions there can also be a collective orientational motion. Tumbling, kayaking, wagging, flow-aligning and log-rolling types of motion have

been observed [11–16]. Here, kayaking is a collective tumbling motion with a non-zero angle of the long colloidal axis with the shear plane. In the wagging state, the inclination angle θ of the nematic director with respect to the flow direction oscillates periodically in the interval $[-\theta_0, \theta_0]$ with $\theta_0 < \pi/2$. Here, some rods are still tumbling, but after tumbling is initiated the majority of them are pushed back by the interactions with their neighbors to a positive inclination angle. In the flow-aligned state, the director is stationary with a positive inclination angle. With increasing shear rate, kayaking turns into wagging and finally into the flow-aligned state [15]. It has been shown that the tumbling frequency depends on the scaled volume fraction $\phi L/d$ and the shear rate, but not on the type of motion [15].

Nematic–isotropic *interfaces* under shear have been studied by molecular dynamics simulations of a model of soft repulsive ellipsoidal particles [17, 18]. Starting from well-equilibrated phase-separated configurations, shear is imposed by Lees–Edwards boundary conditions along the director of the nematically ordered ellipsoids and transverse to that director (log-rolling state), respectively. When the director is aligned with the flow, shear banding is observed, with a higher shear rate in the nematically ordered phase and a lower shear rate in the isotropic (paranematic) phase. Moreover, the determined phase diagram displays nematic–isotropic coexistence with densities essentially unaffected by shear below a threshold shear rate, in contrast to theoretical predictions based on constitutive equations [19, 20], which show that the two-phase region closes with increasing $\dot{\gamma}$. Above this threshold, phase coexistence disappears and the whole systems becomes paranematic.

Experimentally, suspensions of rod-like colloids in shear flow have been studied mainly with *fd* viruses in aqueous solution, where dextran is added as a depletion agent [21]. In particular, the non-equilibrium phase diagram of *fd* viruses has been determined by rheological measurements. These studies yield a strong shear rate dependence of the location of the binodal [21], in contrast to the simulations of [17, 18].

Phase separation under shear is a very complex problem. Already for a simpler system of a phase-separating binary fluid, it is not known whether coarsening after a quench from the homogeneous phase into the two-phase-coexistence region continues indefinitely, as it does without shear, or whether a steady state is reached, in which the fluid domains are strongly elongated in the flow direction, and are characterized by finite length scales ξ_x, ξ_y and ξ_z in the flow, gradient and vorticity directions, respectively [22]. Recent lattice Boltzmann simulations of phase separation in two dimensions indicate that indeed a non-equilibrium steady state (NESS) is reached [23, 24], where the domain sizes are found to scale as $\xi_x \sim \dot{\gamma}^{-2/3}$ and $\xi_y \sim \dot{\gamma}^{-3/4}$ [24]. It remains to be shown whether the same NESS would also be attained after a quench from a macroscopically phase-separated state at rest. In the case of isotropic–nematic coexistence, we expect the domain sizes to be strongly affected by the nematic order.

Hydrodynamic interactions strongly influence or even dominate the dynamical behavior of dilute or semidilute polymeric and colloidal systems [9]. An efficient treatment of the long-range hydrodynamic interactions calls for a coarse-grained and simplified description of the solvent dynamics in order to bridge the large length- and timescale gap between the solvent molecules and the colloid solutes. *A priori*, it is not evident to what extent the colloid dynamics in the isotropic–nematic coexistence regime is affected by hydrodynamic interactions. For a full account of all interactions, however, it is desirable to adopt a theoretical description, which includes hydrodynamic interactions.

In this paper, we investigate the behavior of a suspension of rod-like colloids *at coexistence* of the isotropic and the nematic phase by mesoscale computer simulations, both in the equilibrium state and under flow. The solvent is described by the multi-particle collision dynamics (MPC) algorithm [25–27] and the colloids are simulated by molecular dynamics. Equilibrium [10, 26, 28, 29] and non-equilibrium [30–32] simulations demonstrate that this approach takes hydrodynamic interactions adequately into account. We consider an attractive interaction among the rod-like colloids. This interaction mimics the depletion interaction due to added polymer in the experimental *fd* virus studies [8, 21]. Using phase-separated initial configurations equilibrated in the absence of shear, we study the stability of the two-phase coexistence with increasing shear rate. Depending on the shear rate and interaction strength, we observe a collective rotational motion of the nematically aligned rods, which degrades in time. Since the isotropic phase is driven by the flow into a paranematic state, it increasingly resembles and finally merges with the nematic phase at large shear rates.

This paper is organized as follows. In section 2 the model and the simulation method are described. The equilibrium properties of the system will be discussed in section 3. The non-equilibrium properties for various interaction strengths will be presented in sections 4, 5 and 6. Section 7 is devoted to dynamical aspects of the nematic phase, section 8 to a discussion of the phase diagram and section 9 summarizes our results.

2. Model and simulation method

A hybrid simulation approach is adopted, which combines molecular dynamic simulations for rod-like colloids with the mesoscale multi-particle collision dynamics (MPC) technique for the solvent [25]. Each rod is composed of N_m monomers, which are connected by the harmonic potential

$$V = \frac{\kappa}{2}\left(|\mathbf{R}_i| - l\right)^2, \tag{1}$$

where $\mathbf{R}_i = \mathbf{r}_i - \mathbf{r}_{i-1}$ is the bond vector between the monomers at $\mathbf{r}_i$ and $\mathbf{r}_{i-1}$, and l is the equilibrium bond length. The bond bending potential

$$V_\mathrm{b} = \frac{\kappa_\mathrm{b}}{2}\left(\mathbf{R}_{i+1} - \mathbf{R}_i\right)^2 \tag{2}$$

provides rigidity to each rod such that the mean square end-to-end distance is $0.98(N_\mathrm{m}-1)^2 l^2$ [10]. Interactions between rods are taken into account by the Lennard-Jones potential:

$$V_\mathrm{LJ} = \begin{cases} 4\epsilon\left[\left(\dfrac{\sigma}{r}\right)^{12} - \left(\dfrac{\sigma}{r}\right)^{6}\right], & r < r_\mathrm{c} \\ 0, & r > r_\mathrm{c}, \end{cases} \tag{3}$$

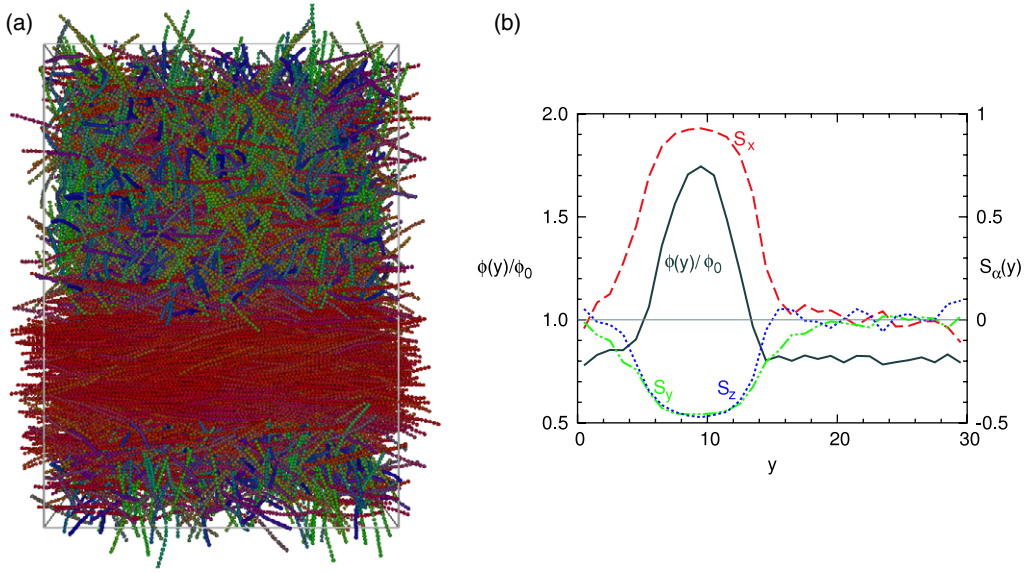

Figure 1. (a) Snapshot of the simulation box with $\epsilon = 3.2k_BT$ at equilibrium in the flow-gradient plane. Colors are coding the rod orientation: left–right direction is red; up–down is green; out-of-plane is blue. (b) Density and orientational order parameter profiles of (a) averaged in planes perpendicular to the y direction. The solid line indicates the normalized packing fraction ϕ/ϕ_0 (left ordinate). Dashed and dotted lines display the orientational order parameter S_α along the gradient direction (right ordinate). The dashed line corresponds to S_x, the dashed–dotted line to S_y and the dotted line to S_z.

with the distance r between monomers and the cutoff radius $r_c = 2.5\sigma$. The parameter ϵ will be varied in order to study the influence of intermolecular interactions on the structure formation and dynamics under shear.

MPC consists of two alternating steps. In the streaming step, solvent particles of mass m move ballistically for a time h. In the collision step, particles are sorted into the cells of a cubic lattice with cell size a, and their velocities relative to the center-of-mass velocity of each cell are rotated by an angle α around a random axis. Monomers are included in the MPC collision step, which accounts for the interaction of rods and solvent. We employ the parameters $\alpha = 150°$, $h = 0.1\sqrt{ma^2/k_BT}$ and $\rho = 50/a^3$ particles per cell. Each rod consists of $N_m = 20$ monomers with the bond length $l = \sigma = 0.25a$, which yields the length $L \approx 5a$, taking end-caps into account. The monomer mass is $M = 12.5m$, which provides an optimal hydrodynamic coupling between the rods and the solvent [33]. We simulate $N_p = 10\,000$ rods in a box of size $(L_x, L_y, L_z) = (22a, 30a, 20a)$. To impose shear flow, Lees–Edwards boundary conditions are employed, which for a homogeneous phase results in a linear velocity profile $(v_x, v_y, v_z) = (\dot\gamma y, 0, 0)$, where y is the position in the gradient direction and $\dot\gamma$ is the shear rate. In order to maintain a constant temperature, we scale the velocities relative to the center-of-mass velocity within a collision cell, i.e. we use a profile-unbiased thermostat [34].

To compare with experimental results and to gain insight into physical mechanisms, it is desirable to express physical quantities in dimensionless units. The Peclet number $Pe = \dot\gamma/D_r$ is the shear rate in units of the rotational diffusion coefficient of the rods. Here, we employ the rotational diffusion coefficient D_r^0 at infinite dilution. This value is generally available in experiments and in simulations. An analytical expression [9, 35] is

$$D_r^0 = \frac{3k_BT}{\pi\eta}\frac{1}{L^3}\left[\ln\left(\frac{L}{d}\right) - \frac{2}{3}\right] \tag{4}$$

for rods of length L and effective diameter d, where η is the solvent viscosity. For the parameters employed in our simulations, we obtain $D_r^0 = 3 \times 10^{-4}\sqrt{k_BT/ma^2}$. In a previous study of the dynamics of a single rod-like colloid in an MPC solvent [10], we found good quantitative agreement between analytical and simulated values of the translational diffusion coefficient (with a deviation of about 20%), and we expect a similar agreement for the rotational diffusion coefficient. With D_r^0, the shear rate $\dot\gamma = 0.001/\sqrt{ma^2/k_BT}$ corresponds to the Peclet number $Pe = 3$.

3. Isotropic–nematic coexistence at equilibrium

Onsager theory and previous simulation results [4, 7] for rods with repulsive interactions indicate that isotropic–nematic phase coexistence can be found in a small interval of packing fractions that depends on the rod aspect ratio. Two main routes are employed to arrive at an equilibrium structure in this density range. Starting from an isotropic orientation, we observe the formation of nematically ordered domains. Alternatively, we start from a purely nematic state, in which all the rods are oriented in the same direction (x), but their centers of mass display fluid-like order. In this case part of the system melts and only a nematic domain remains. After equilibration, systems with various initial conditions are approximately equivalent.

A typical snapshot of an equilibrium state obtained by melting a nematic initial structure is shown in figure 1(a). The suspension is separated into two easily distinguishable regions.

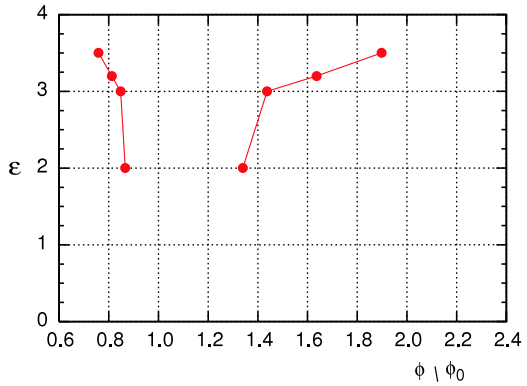

Figure 2. Phase diagram of colloidal rods with aspect ratio $L/d = 20$ as a function of the strength ϵ of the attractive interaction.

In the isotropic phase rods are oriented in all spatial directions with equal probability. Rods in the nematic phase are mostly aligned parallel to the interface.

The orientational order parameter with respect to a direction $\mathbf{u}_\alpha$ in space is defined as

$$S_\alpha = \tfrac{1}{2}\left\langle 3\cos^2\theta - 1\right\rangle, \tag{5}$$

where θ is the angle between the rod director and the direction $\mathbf{u}_\alpha$. For rods aligned along $\mathbf{u}_\alpha$, $S_\alpha = 1$, rods aligned in the perpendicular direction yield $S_\alpha = -0.5$, and in the case of isotropic orientations, $S_\alpha = 0$.

In order to analyze the density and order parameter difference between the coexisting phases, we average the center-of-mass positions and the orientations of the rods in slices of thickness a perpendicular to the gradient direction y. Figure 1(b) shows the packing fraction ϕ, normalized by the average value ϕ_0, and the orientational order parameters S_α for the three orthogonal directions. The isotropic phase is characterized by a density lower than ϕ_0 and by the three S_α fluctuating around zero. In the nematic phase instead, the density is larger than ϕ_0 and three distinct values of the order parameter are obtained. These are close to unity along the nematic director (S_x) and close to -0.5 in both perpendicular directions (S_y and S_z).

From simulations for various interaction strengths ϵ, we can construct the phase diagram shown in figure 2. The two-phase-coexistence region is found to widen with increasing ϵ, as expected. More interestingly, the simulations show that the density difference of the coexisting isotropic and nematic phases increases weakly for $\epsilon \lesssim 3k_BT$, while it increases very strongly for larger interaction strengths.

This dependence very much resembles the behavior observed experimentally in suspensions of *fd* viruses with dextran as a depletion agent [8]. For small polymer concentrations, the phase behavior is only weakly affected, but the gap of the colloid volume fractions of the coexisting isotropic and nematic phases becomes very large for high polymer concentrations. Here, it is important to emphasize a difference between our way of modeling attractive interactions by a Lennard-Jones potential and a polymer-induced depletion interaction. The polymers do not partition equally in the two coexisting phases, but are enriched in the isotropic phase of low colloid volume fraction [8]. Therefore, in the experimental system the depletion attraction is stronger in the isotropic than in the nematic phase—while it is the same in the simulation model.

4. Coexistence under shear flow for moderate attraction

The shear flow is applied in the direction of the nematic director of the equilibrium state. It is important to note that Lees–Edwards boundary conditions enforce only a total velocity difference across the system in the gradient (y) direction, while the actual velocity profile is a consequence of how the system adapts to the flow. In the case of a simple fluid this profile is linear, while in the presence of colloidal or polymeric particles different profiles are obtained, as has been shown in [36] for a star polymer in solution.

Various systems with coexisting phases in a shear flow have been shown to display shear banding [37–39], i.e. different shear rates develop in the coexisting phases as a consequence of their different viscosities of the system in the coexisting phases. Such phenomena would therefore be expected in our initially isotropic nematic separated system. However, within the accuracy of our data, we find that the velocity profile is approximately linear, with one unique slope, along the gradient direction. This is in contrast to results of MD simulations for ellipsoidal particles without solvent, where shear banding has been found [18]. The presence of an explicit solvent with non-zero viscosity η_0 reduces the effect of rod-like particles on the total viscosity. As a result, the viscosity difference and consequently the difference in the shear rates in our simulations becomes too small to be detected.

One of the two main mechanisms induced by shear in the concentrated rod solution is that rods tend to align with the flow in the initially isotropic phase. This phase is usually referred to as paranematic. The induced orientational order generates a free volume around each rod which facilitates the *densification* of the paranematic phase. Consequently, rods initially placed in the nematic layer will slowly move into the paranematic region, which results in an *erosion* of the nematic phase, so that the difference in density between the two phases decreases with increasing shear rate.

An example of a state with coexisting paranematic and nematic phases (PN–N) is presented in figure 3. The snapshot of figure 3(a) shows qualitatively that the initially nematic layer is less compact and less oriented with the nematic director than in equilibrium. Complementary, the paranematic layer has a noticeable proportion of rods aligned with the flow. The density averages in figure 3(b) quantitatively show the difference between the two phases: density and order parameter in the flow direction are higher in the nematic phase (region around $y = 9$) than in the paranematic phase (region around $y = 25$).

The second main mechanism induced by the applied shear flow is a rotational motion, which in the dense suspension that we are dealing with emerges as a collective phenomenon. The rotation of individual rods is observed in both phases.

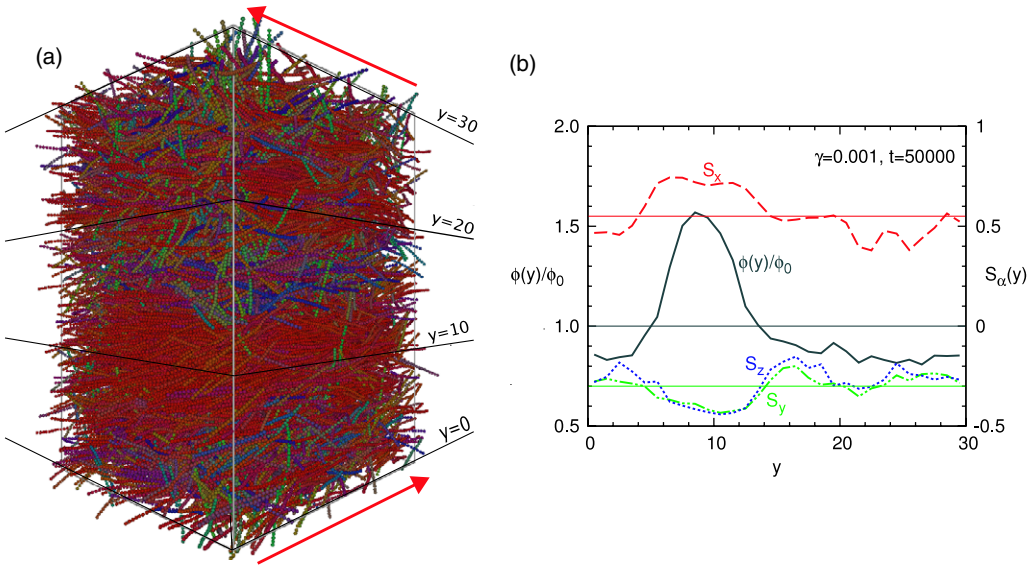

Figure 3. Snapshot of a coexisting state with a paranematic and a nematic flow-oriented phase, corresponding to $\epsilon = 3.2k_BT$, $\dot{\gamma} = 0.001/\sqrt{ma^2/k_BT}$ and $\dot{\gamma}t = 50.0$. (a) Snapshot and (b) average density and orientational order parameter. Color codes and line types are the same as in figure 1. Red arrows in (a) indicate the direction of the flow and black lines show the gradient scale in order to compare with (b).

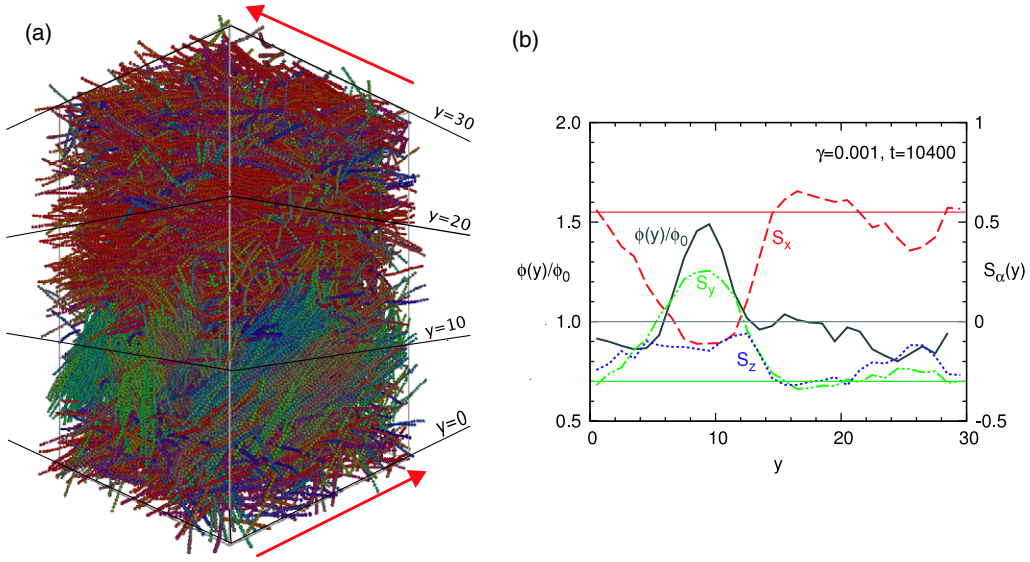

Figure 4. Snapshot of a coexisting state with a flow-oriented paranematic phase and a nematic phase undergoing a collective rotation, corresponding to $\epsilon = 3.2k_BT$, $\dot{\gamma} = 0.001/\sqrt{ma^2/k_BT}$ and $\dot{\gamma}t = 10.4$. (a) Snapshot and (b) computed averages with the same color code as in figure 1.

However, in the initially nematic phase, large or very large clusters of rods are observed to simultaneously rotate. An example of a system undergoing a collective rotation is shown in figure 4. In the snapshot of figure 4(a), the upper part of the system remains aligned with the flow direction, quite similar to the corresponding region in figure 3(a). In contrast, the rods in the lower region are mainly aligned with the gradient direction, i.e. perpendicular to the flow. Figure 3(b) shows that the density remains higher in the initially nematic part of the system, while the director at this particular moment points mainly in the gradient direction. As the tumbling motion proceeds, the director continues its motion until most rods are again aligned with the flow direction. This aligned state is energetically and entropically favorable for the rods and also minimizes the torque on the rods induced by the flow. Therefore, rods are, for a much longer time, aligned with the flow than perpendicular to it, as can be observed in figures 5(b) and (c).

In order to better understand the dynamical behavior of the two coexisting phases, it is instructive to investigate the density and orientational order parameter averages as a function of time. In figures 5(a) and (b), the normalized packing fraction

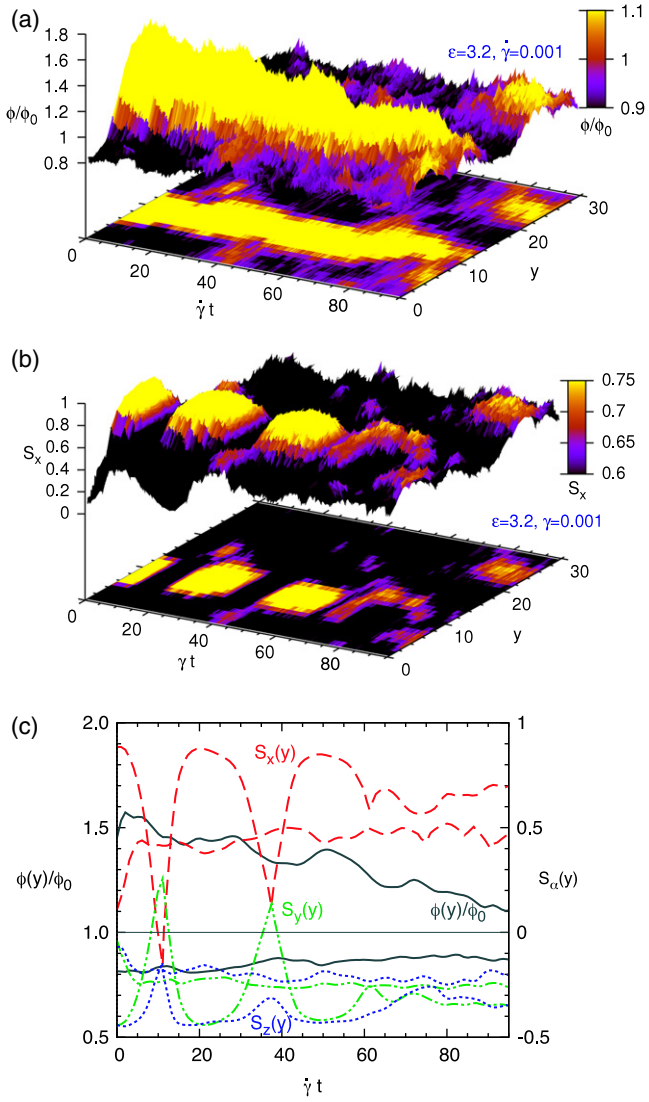

Figure 5. Time dependence of the normalized packing fraction ϕ/ϕ_0 and orientational order parameters S_α for $\epsilon = 3.2k_BT$ and $\dot{\gamma} = 0.001/\sqrt{ma^2/k_BT}$. (a) and (b) are a three-dimensional representation of the computed averages along the gradient direction y as a function of time, with values represented with a color code displayed in the legend. (c) Time evolution of ϕ/ϕ_0 and S_α in two gradient locations corresponding to the initial separated isotropic and nematic phases. Similar to previous figures, solid lines account for the normalized packing fraction ϕ/ϕ_0 and discontinuous lines for the orientational order parameter S_α along the gradient direction. Dashed lines correspond to S_x, dashed–dotted lines to S_y and dotted lines to S_z.

ϕ/ϕ_0 and the orientational order parameter S_x in the flow direction are displayed as a function of time. The projection into the time-gradient plane of the average values of ϕ/ϕ_0 and S_x is also shown. The time origin corresponds to the moment when the shear flow is switched on, starting from an equilibrium configuration. In figure 5(a), the erosion of the initially nematic phase can be observed, together with the corresponding densification of the initial isotropic phase. In figure 5(b), the tumbling dynamics of the nematic phase is reflected in the consecutive maxima and minima of S_x, where the nematic phase is aligned with and perpendicular to the flow, respectively. Note that figures 3 and 4 present snapshots at $\dot{\gamma}t = 10.4$ and $\dot{\gamma}t = 50$ of figure 5.

To characterize the tumbling-nematic and paranematic phases, we determine their positions by the maximum and minimum of the density profile $\phi(y)$, respectively. To reduce the effect of thermal fluctuations, we average the densities and orientational order parameter over three neighboring slices (of thickness a). The normalized volume fraction ϕ/ϕ_0 and the three components of S_α obtained in this way are displayed for both phases as a function of time in figure 5(c). The orientational order parameter in the three directions clearly shows the tumbling motion in this phase. The rod orientation shows consecutive minima that coincide in time with maxima of the orientational order parameter in both the gradient and the vorticity directions. The actual values of the orientational order parameter at these maxima are related with the size of the region that simultaneously rotates, which is decreasing in time. The initially well-phase-separated system yields a well-defined rotation of the whole nematic band at early times. Nevertheless, at later times the system may lose synchronicity as can be seen in figures 5(a)–(c). This occurs for all the shear rates analyzed in the case of the attraction strength $\epsilon = 3.2k_BT$.

In order to understand this behavior at longer times, several points have to be considered. First, note that the values presented in figure 5 are calculated by averaging the rod positions and orientations in slices perpendicular to the gradient direction. This implies that in an inhomogeneous layer small variations are averaged out, for example in the case when only a small group of rods undergoes a rotation. The differences in density and orientational order parameter between the two coexisting phases are then clearly underestimated in figure 5(c). We infer from this analysis that the size of the cluster that rotates collectively is initially larger than the system size, and becomes smaller with time. It can also be seen that this region does not remain in a fixed position in space, but can shift or split in more than one region, or even dilute and emerge in a separate part of the system (see $\dot{\gamma}t \simeq 90$ in figures 5(a) and (b)). It will be shown in section 6 that the size of the tumbling-nematic region varies with the strength of the attraction. The existence of small regions of higher densities and larger order parameters can also be observed in figures 5(a) and (b). These regions are separated from the main tumbling-nematic phase and, in the current case, exist for short times only.

Transient oscillations of the shear viscosity have been observed experimentally in step-down shear-jump and flow-reversal experiments [21]. These experiments were conducted mainly in the nematic phase and show a strong damping both in the flow-aligning and the tumbling regimes, but a weak damping at the border between these two regimes. The decay of the oscillations is interpreted by a loss of coherence in the tumbling motion of different domains. This is consistent with the decay of oscillations of the nematic order parameter in our simulations, see figure 5.

The time evolution of the packing fraction (dark solid line in figure 5(c)) shows a slower relaxation than for the orientational order parameters. The origin is easy to

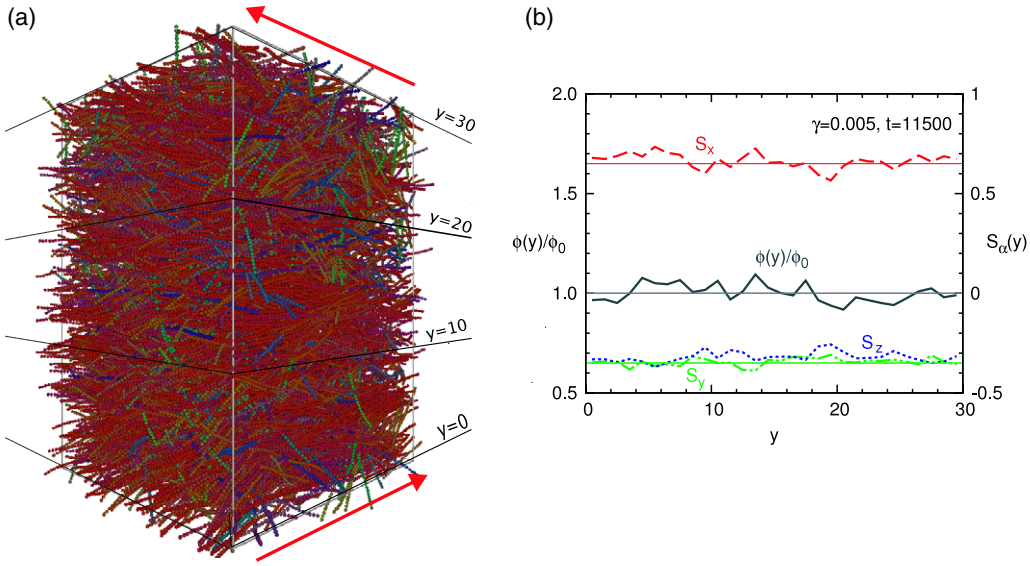

Figure 6. Snapshot of a homogeneous shear-induced state, corresponding to $\epsilon = 3.2k_BT$, $\dot{\gamma} = 0.005/\sqrt{ma^2/k_BT}$ and $t = 11500\sqrt{ma^2/k_BT}$ ($\dot{\gamma}t = 10.4$). (a) Snapshot and (b) computed averages with the same color code as in figure 1.

understand. The alignment of the rods in the isotropic phase takes place first and it is the new available free space that facilitates the rods' spatial redistribution of rods.

In the tumbling-nematic phase, the packing fraction decreases slowly in the available time window and shows periodic modulations induced by the tumbling motion of the rods. This decrease in density is most likely caused by a loss of coherence in the rotation of the rods within the collectively tumbling clusters as mentioned above.

The simulations presented here correspond to the attraction parameter $\epsilon = 3.2k_BT$, although the initial configuration corresponds to the equilibrium isotropic–nematic state at $\epsilon = 3.0k_BT$. This is the explanation for the small increase of the density in the nematic phase at very short times that can be observed in figure 5(c). Also interesting is the increase of the order parameter in the vorticity direction during the rotation events that can be seen in figure 5(c), which corresponds to kayaking motion [15] (i.e. the rotation of the rods does not occur in the gradient-flow plane but tilts also in the vorticity direction).

In contrast to this rich behavior of the tumbling-nematic phase, the paranematic area of the system shows a much smoother behavior in which the relevant quantities fluctuate around a final steady-state value and no collective rotation is seen.

5. High shear rates

As the shear rate increases, the differences between the two phases decrease, and for shear rates exceeding a critical value $\dot{\gamma}_{max}$, a single paranematic phase is obtained.

Figure 6 displays an example of such a state. The snapshot shows that the separation between the phases is lost and the density and orientational order are approximately homogeneous across the whole simulation box. The time evolution from the initially phase-separated system into the final state is presented in figure 7. The dynamics of the initially nematic region displays a much less rich behavior than in the case of moderate shear rates. Although a transient oscillatory component of S_x is still visible in figures 7(b) and (c), it decays rapidly and S_x becomes stationary. These short-time oscillations can either be due to a transient wagging behavior or due to tumbling of small clusters of rods in the initially nematic band. In any case, the time dependence in figure 7 shows unequivocally the merging of the two phases.

The density and order parameter profiles presented in figure 6(b) show fluctuations around a homogeneous value, as a consequence of averaging in planes perpendicular to the gradient direction. These fluctuations are responsible for the remaining density differences at late times in figure 7(c). As explained in section 4, the time evolution of the initially coexisting phases plotted in figure 7(c) are obtained by identifying the two slices in which the density assumes the highest and lowest values. This implies that the two extreme densities will remain different even in the homogeneous state. Therefore, with this criterion, coexisting phases have to have a density difference of larger than 5% in order to be distinguishable.

Finally, we want to mention that the flow alignment in the paranematic phase increases with increasing shear rate, as indicated by the increase from $S_x \simeq 0.55$ at $\dot{\gamma} = 0.001/\sqrt{ma^2/k_BT}$ to $S_x \simeq 0.65$ at $\dot{\gamma} = 0.005/\sqrt{ma^2/k_BT}$ (see figure 6(b)).

6. Coexistence under shear flow for strong attraction

A much more pronounced density difference of the coexisting isotropic and nematic phases is obtained for higher interaction strength, $\epsilon = 4.0k_BT$. Simulation results at the shear rate $\dot{\gamma} = 0.007/\sqrt{ma^2/k_BT}$ are shown in figure 8. As initial

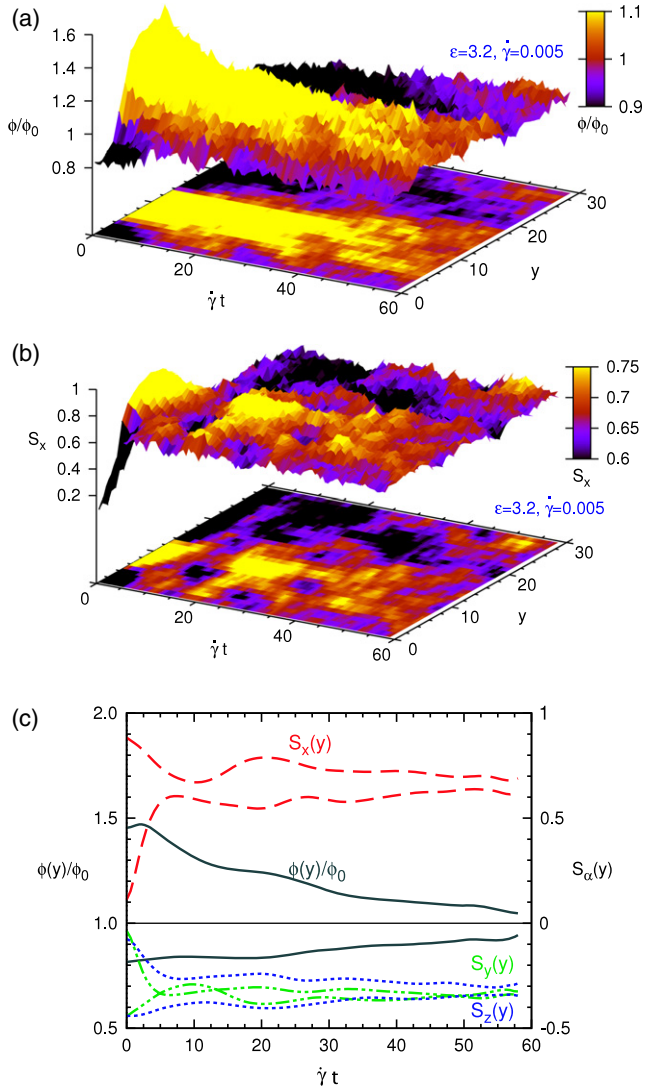

Figure 7. Time dependence of ϕ/ϕ_0 and S_α for $\epsilon = 3.2k_BT$ and $\dot\gamma = 0.005/\sqrt{ma^2/k_BT}$. The line types are defined in figure 5.

condition, we employ an equilibrated system at $\epsilon = 3.0k_BT$. In contrast to the smaller ϵ, the nematic phase is now very stable under flow. This is evident from figure 8(b), where the density of the nematic phase first increases and then saturates as a function of time. Simultaneously, the amplitude of the order parameter oscillations increases, see figures 8(a), (b). Thus, the rods in the nematic region remain well aligned during the tumbling process. An interesting difference to the results for $\epsilon = 3.2k_BT$ is that the kayaking motion occurs now almost completely in the shear-vorticity plane, since the amplitude of S_y is smaller than that of S_z, see figure 8(b). This type of kayaking motion appears for all shear rates at this interaction strength. However, we observe a decrease in the density difference and the order parameter with time for $\dot\gamma = 0.009/\sqrt{ma^2/k_BT}$.

We conclude that, for $\epsilon = 4.0k_BT$ and $\dot\gamma = 0.007/\sqrt{ma^2/k_BT}$, the size of the nematic domain rotating coherently is larger than the size of our simulation box, so that the nematic layer remains stable.

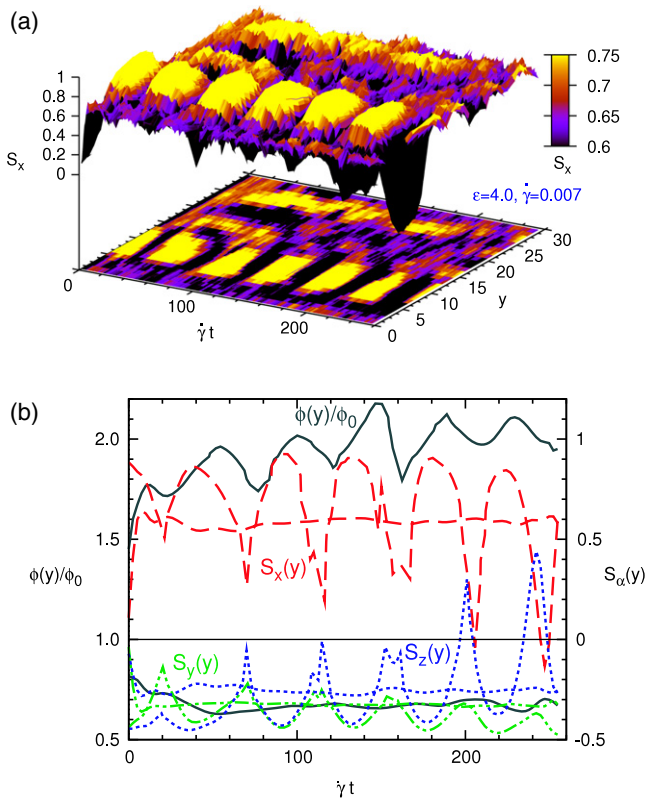

Figure 8. Time dependence of ϕ/ϕ_0 and S_α for $\epsilon = 4.0k_BT$ and $\dot\gamma = 0.007/\sqrt{ma^2/k_BT}$. Color code and line types are defined in figure 5.

As for $\epsilon = 3.2k_BT$ at $\dot\gamma = 0.001/\sqrt{ma^2/k_BT}$, we observe clusters of higher density and orientational order in the paranematic phase, which now exhibit a large lifetime (see figure 5).

7. Tumbling times

The periodic motion of the nematic director during tumbling and kayaking is characterized by a time τ between subsequent flow-aligned states. To determine this typical time is a non-trivial task. In section 4, we have extensively discussed our observations regarding the loss of synchronicity in the tumbling-nematic phase. Namely, that different regions or clusters inside the tumbling-nematic phase may tumble at different times, split in more than one region or dissolve and nucleate in a separate part of the main nematic domain. These considerations make the definition of τ not unique. Ideally, in the case that the oscillations are well developed, τ can be determined as the time between the two deepest minima of the order parameter $S_x(t)$ in the flow direction. This is possible only in some cases, for example for $\epsilon = 3.2k_BT$ and $\dot\gamma = 0.001/\sqrt{ma^2/k_BT}$, for times such that $\dot\gamma t \leqslant 50$ (see figure 5(c)). Alternatively, we use the time at which $S_{x(t)}$ reaches its first minimum after flow has been switched on, which is equivalent to $\tau/2$. In the equilibrium state, all rods in the nematic phase are well aligned, such that a synchronous collective rotation is induced after flow has been switched on for most of the parameter sets.

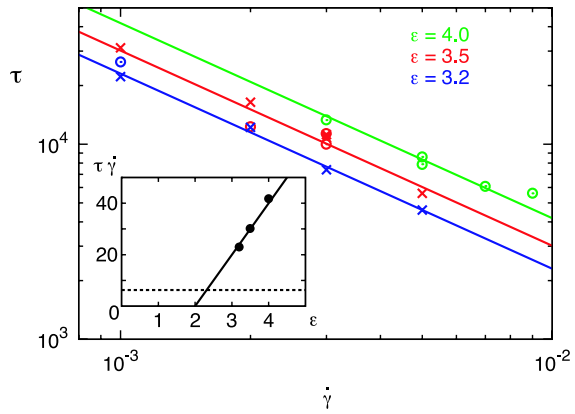

Figure 9. Tumbling times τ (in units of $\sqrt{ma^2/k_BT}$) as a function of shear rate $\dot\gamma$ for the interaction strengths $\epsilon = 3.2k_BT$, $3.5k_BT$ and $4k_BT$ (bottom to top). The lines reflect the $1/\dot\gamma$ dependence. The crosses denote tumbling times determined by the time between successive minima of the orientational order parameter S_x and the circles the tumbling times defined by the first minimum of S_x after shear has been switched on. The inset shows the dependence of $\dot\gamma\tau$ on the interaction strength. The solid line is a linear extrapolation and the dotted line corresponds to the dilute limit where $\dot\gamma\tau = 2\pi$.

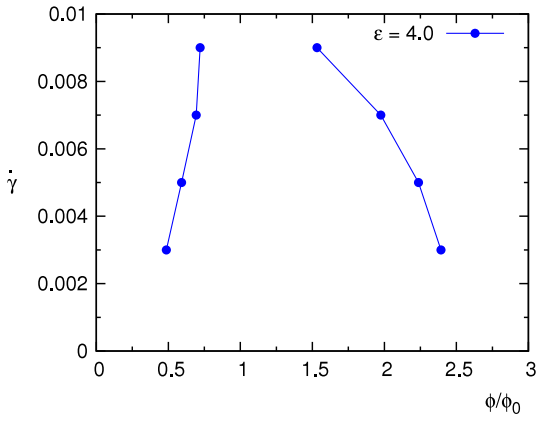

Figure 10. Coexistence region between paranematic and tumbling-nematic phases as a function of the shear rate $\dot\gamma$, for the attraction strength $\epsilon = 4.0k_BT$. Symbols correspond to simulation results.

The results for the tumbling times are shown as a function of the shear rate in figure 9. First we see that the two ways described of estimating τ give consistent results. For strong attraction, $\epsilon = 4.0k_BT$, the second estimate is less reliable, since we start the simulation with an equilibrium configuration for $\epsilon = 3.0k_BT$; thus, this way of estimating τ is not used in this case. Furthermore, we find that the tumbling time decreases linearly with the shear rate $\dot\gamma$, in good agreement with simulations [15] and experiments [40] well inside the nematic phase. Interestingly, the value of $\dot\gamma\tau$ depends on the interaction strength. Our results displayed in figure 9 demonstrate that the tumbling time increases with increasing ϵ. We believe that this is due to the higher packing fraction of rods in the nematic phase. This implies that the distance between rods is smaller, and therefore the hydrodynamic friction for their motion parallel to each other is larger.

8. Phase diagram

The non-equilibrium phase diagram of the system of attractive rod-like colloids in flow can now be determined by plotting the densities of the coexisting nematic and paranematic phases for various shear rates with $\dot\gamma < \dot\gamma_{max}$. Our results for $\epsilon = 4.0k_BT$ and for $\epsilon = 3.2k_BT$ are presented in figures 10 and 12, respectively.

We first consider the case of large attraction, i.e. $\epsilon = 4.0k_BT$. In this case, it is possible to reach a stationary coexistence state of a flow-aligned paranematic and a tumbling-nematic phase within the accessible time range of $\dot\gamma t \leqslant 100$, as shown in figure 8. The phase diagram shows a densification of the paranematic and the erosion of the nematic phase with increasing shear rate, in qualitative agreement with the experimental results of [21]. As pointed out in section 6, we observe a decrease in the density difference between the coexisting phases for $\dot\gamma = 0.009/\sqrt{ma^2/k_BT}$. Hence, we expect that the maximum shear rate, at which there will be a paranematic phase only, is only slightly larger than $\dot\gamma = 0.01/\sqrt{ma^2/k_BT}$.

The situation is more complex for moderate attractions. The time dependence of the density and the order parameter shown in figure 5 indicates that order in the nematic layer is slowly lost. This can have several reasons. It can be due to a correlation length of coherent kayaking motions, which is smaller than the size of our simulation box. An indication of such nematic domains can indeed be seen already at an early time of $\dot\gamma t = 10.4$ in figure 4. A decay of oscillations in the viscosity after flow reversal observed in [21] can be attributed to this kind of decorrelation. It is also possible that the complicated, time-dependent flow pattern in phase-separated binary mixtures, with large fluctuations in the domain sizes, leads to an intermittent destruction and reappearance of the nematic order as that observed in figures 5(a) and (b).

Furthermore, the thickness of the nematic layer can be very important. We have considered a packing fraction of rods, for which roughly a quarter of the box is occupied by a nematic layer. The thickness of this nematic layer corresponds to about two rod lengths. Thus, the interface region and the bulk-nematic region is similar in size, see figure 1, which may destabilize the nematic layer under shear. It is conceivable that a thicker nematic layer is considerably more stable under flow.

For the current simulations, we estimate the shape of the phase diagram in the case of moderate attractions in the following way. Starting from an equilibrium state, shear causes an increase in the density of the initially isotropic phase. This density assumes, after some time, a stationary value. We determine the time t_s when this stationary state has been reached. The densities in the vicinity of this time represent the densities of the coexisting phases. To account for the modulations in the density of the initially nematic phase by the tumbling, we calculate the density of the coexisting nematic phase by averaging the density of this phase over a suitable time interval in the vicinity of t_s. In figure 11 these time intervals are indicated for $\epsilon = 3.2k_BT$. It can be seen that $\dot\gamma t_s \simeq 40$ for all simulated shear rates. However, the

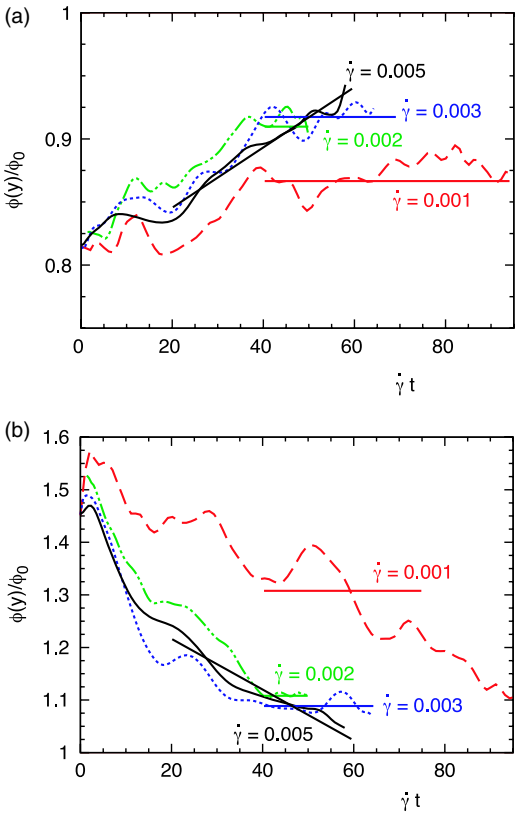

Figure 11. Time evolution of the normalized density ϕ/ϕ_0 for various shear rates for the attraction strength $\epsilon = 3.2k_BT$ in (a) the initially isotropic phase and (b) the initially nematic phase. Values of the shear rates are indicated in the figure. The straight lines show the time over which averages have been performed. Note that for the largest shear rate a stationary value has not been reached.

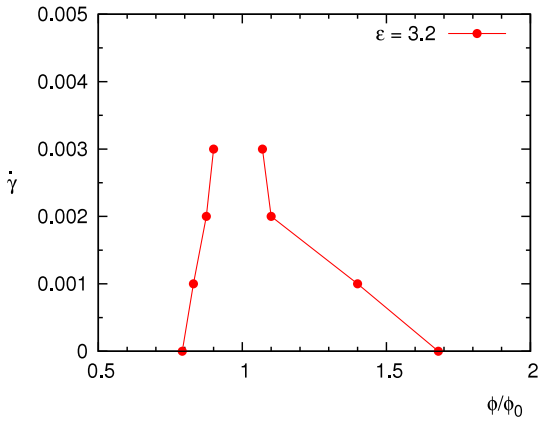

Figure 12. Diagram of the phase separation between paranematic and tumbling-nematic states as a function of the shear rate $\dot\gamma$, for moderate attraction, $\epsilon = 3.2k_BT$. Symbols correspond to simulation results.

behavior for $\dot\gamma = 0.005/\sqrt{ma^2/k_BT}$ is different as a plateau is not reached within the simulation time. This is in agreement with the estimate that $\dot\gamma_{max} < 0.005/\sqrt{ma^2/k_BT}$ and $\dot\gamma_{max} > 0.003/\sqrt{ma^2/k_BT}$. This approach yields the phase diagram presented in figure 12.

We believe that the definition of an effective phase diagram—by assigning a particular time $\dot\gamma t$ after switching on the flow or after flow reversal—is not only useful for the interpretation of simulation results, but can also be useful for a detailed comparison with experiment. This is interesting, because the typical timescales in experiments [21] are similar to those accessible in simulations.

9. Summary and conclusions

We have investigated, by mesoscale computer simulations, the effect of shear flow on a suspension of rod-like colloids that, in equilibrium, displays an isotropic–nematic coexistence. We have first determined the equilibrium phase diagram as a function of the strength of an attractive interaction between the colloidal particles. We find a widening of the two-phase-coexistence region, which is weak for interaction strengths $\epsilon \leqslant 3.0k_BT$, but becomes very pronounced for stronger interactions.

Shear flow orients the particles in the initially isotropic phase. This generates free space and facilitates the transfer of rods from the nematic into the paranematic layer. This mechanism is responsible for the reduction of the density difference between the two phases. Shear flow also induces a rotational motion of individual rods. More interestingly, it leads to a collective rotational motion of large groups of rods in the nematic phase. We have determined the characteristic timescale of this collective tumbling motion and find that it decreases linearly with the inverse shear rate, as observed previously well inside the nematic region. Furthermore, we observe that the tumbling time increases with increasing interaction strength. In contrast, the paranematic phase remains flow-aligned without any collective motions.

We construct phase diagrams as a function of colloidal volume fraction and shear rate, either by using the long-time stationary states obtained in our simulations, or by defining an effective phase-coexistence region by employing the densities at a fixed time $\dot\gamma$ after switching on the flow. Support for the simulated phase behavior comes from the comparison with experimental measurements obtained with *fd* viruses in suspensions with dextran polymer [21]. The addition of polymer induces a depletion interaction between the colloids, which can be mimicked by our model with attractive interactions.

In order to confirm our results, and to investigate the issue of phase separation under flow in more detail, larger system sizes and longer simulation times are necessary. Such large-scale simulations come into reach with the availability of modern, massively parallel computer architectures.

Acknowledgments

We thank M P Lettinga and J K G Dhont for many helpful and stimulating discussions. Financial support by the German Research Foundation (DFG) within SFB TR6, and the European Network of Excellence 'SoftComp' (contract NMP3-CT-2004-502235) is gratefully acknowledged. MR also thanks the Spanish MCYT (project FIS2007-65869-C03-03)

for partial support. We are grateful to the John von Neumann Institute for Computing (NIC) at the Research Centre Jülich for a generous allocation of computer time.

References

[1] Chaikin P M and Lubensky T C 1995 *Principles of Condensed Matter Physics* (Cambridge: Cambridge University Press)
[2] Vroege G J and Lekkerkerker H N W 1992 *Rep. Prog. Phys.* **55** 1241
[3] Cuetos A and Dijkstra M 2006 *Phys. Rev. Lett.* **98** 095701
[4] Onsager L 1949 *Ann. New York Acad. Sci.* **51** 627
[5] Khokhlov A R and Semenov A N 1982 *Physica* A **112** 605
[6] Dijkstra M and Frenkel D 1995 *Phys. Rev.* E **51** 5891
[7] Fynewever H and Yethiraj A 1997 *J. Chem. Phys.* **108** 1636
[8] Dogic Z, Purdy K R, Grelet E, Adams M and Fraden S 2004 *Phys. Rev.* E **69** 051702
[9] Doi M and Edwards S F 1986 *The Theory of Polymer Dynamics* (Oxford: Clarendon)
[10] Winkler R G, Mussawisade K, Ripoll M and Gompper G 2004 *J. Phys.: Condens. Matter* **16** S3941
[11] Larson R G and Öttingger H C 1991 *Macromolecules* **24** 6270
[12] Faraoni V, Grosso M, Crescitelli S and Maffettone P L 1999 *J. Rheol.* **43** 829
[13] Hess S and Kröger M 2004 *J. Phys.: Condens. Matter* **16** S3835
[14] Kröger M 2004 *Phys. Rep.* **390** 453
[15] Tao Y-G, den Otter W K and Briels W J 2005 *Phys. Rev. Lett.* **95** 237802
[16] Tao Y-G, den Otter W K and Briel W J 2006 *J. Chem. Phys.* **124** 204902
[17] Germano G and Schmid F 2003 *NIC Symp. 2004* (*NIC Series* vol 20) ed D Wolf, G Münster and M Kremer (Jülich: John von Neumann Institute for Computing) pp 311–20
[18] Germano G and Schmid F 2005 *J. Chem. Phys.* **123** 214703
[19] Olmsted P D and Lu C-Y D 1997 *Phys. Rev.* E **56** R55
[20] Dhont J K G and Briels W J 2006 *Soft Matter* (*Complex Colloidal Suspensions* vol 2) ed G Gompper and M Schick (Weinheim: Wiley–VCH) pp 147–283
[21] Lettinga M P and Dhont J K G 2004 *J. Phys.: Condens. Matter* **16** S3929
[22] Onuki A 2002 *Phase Transition Dynamics* (Cambridge: Cambridge University Press)
[23] Wagner A J and Yeomans J M 1999 *Phys. Rev.* E **59** 4366
[24] Stansell P, Stratford K, Desplat J-C, Adhikari R and Cates M E 2006 *Phys. Rev. Lett.* **96** 085701
[25] Malevanets A and Kapral R 1999 *J. Chem. Phys.* **110** 8605
[26] Malevanets A and Kapral R 2000 *J. Chem. Phys.* **112** 7260
[27] Ihle T and Kroll D M 2001 *Phys. Rev.* E **63** 020201(R)
[28] Ripoll M, Mussawisade K, Winkler R G and Gompper G 2004 *Europhys. Lett.* **68** 106
[29] Mussawisade K, Ripoll M, Winkler R G and Gompper G 2005 *J. Chem. Phys.* **123** 144905
[30] Noguchi H and Gompper G 2004 *Phys. Rev. Lett.* **93** 258102
[31] Noguchi H and Gompper G 2005 *Proc. Natl Acad. Sci. USA* **102** 14159
[32] Ripoll M, Winkler R G and Gompper G 2006 *Phys. Rev. Lett.* **96** 188302
[33] Ripoll M, Mussawisade K, Winkler R G and Gompper G 2005 *Phys. Rev.* E **72** 016701
[34] Evans D J and Morriss G P 1990 *Statistical Mechanics of Nonequilibrium Fluids* (San Diego, CA: Academic)
[35] Tirado M M and Garcia de la Torre J 1980 *J. Chem. Phys.* **73** 1986
[36] Ripoll M, Winkler R G and Gompper G 2007 *Eur. Phys. J.* E **23** 349
[37] Berret J F, Porte G and Decruppe J F 1997 *Phys. Rev.* E **55** 1668
[38] van der Gucht J, Lemmers M, Knoben W, Besseling N A M and Lettinga M P 2006 *Phys. Rev. Lett.* **97** 108301
[39] Dhont J K G and Briels W J 2008 *Rheol. Acta* **47** 257
[40] Lettinga M P, Dogic Z, Wang H and Vermant J 2005 *Langmuir* **21** 8048